

Enhancing cross-polarisation discrimination or axial ratio beamwidth of diagonally dual or circularly polarised base station antennas by using vertical parasitic elements

ISSN 1751-8725
 Received on 24th October 2016
 Revised 15th January 2017
 Accepted on 12th February 2017
 E-First on 19th June 2017
 doi: 10.1049/iet-map.2016.0928
 www.ietdl.org

Yu Luo^{1,2} ✉, Qing-Xin Chu¹, Jens Bornemann³

¹School of Electronic and Information Engineering, South China University of Technology, Guangzhou 510641, People's Republic of China

²Department of Electrical and Computer Engineering, National University of Singapore, Singapore 117583, Singapore

³Department of Electrical and Computer Engineering, University of Victoria, PO Box 1700 STN CSC, Victoria, BC, Canada V8W 2Y2

✉ E-mail: elelyu@nus.edu.sg

Abstract: The cross-polarisation discrimination (XPD) of a $\pm 45^\circ$ dual-polarised base station antenna is enhanced by adding vertical parasitic elements. First, it is established that high XPD can be achieved by employing four vertical parasitic elements between a simple $\pm 45^\circ$ dual-polarised radiator and ground. Second, based on the proposed method, a simple $\pm 45^\circ$ dual-polarised antenna for a long-term evolution 1.71–2.17 GHz base station is designed, fabricated and measured. Compared with the antenna without vertical elements, XPDs are improved by about 7 dB in the horizontal plane due to the addition of the vertical parasitic elements. Third, with a wideband quadrature hybrid, the proposed antenna is shown to radiate circularly polarised waves. In particular, the 3 dB axial ratio beamwidth of the proposed antenna is increased from 84° to 195° with the addition of the four vertical parasitic elements.

1 Introduction

Due to their attractive features and advantages, polarisation diversity techniques have been widely used in modern mobile communication systems. $\pm 45^\circ$ dual-polarised base station antennas are widely applied to combat multipath propagation effects and to enhance signal reception quality [1, 2]. The cross-polarisation discrimination (XPD) is a crucial technical indicator to evaluate the performance of base station antennas following Ludwig's third definition [3]. Current technical standards, as set, e.g. by China Mobile Ltd call for XPD better than 20 dB at boresight and better than 10 dB within $\pm 60^\circ$ of the main lobe.

Previous studies on $\pm 45^\circ$ dual-polarised antennas, e.g. [4–9], are mainly concerned with impedance matching, simple structures, beamwidth, isolation between two ports, low cross-polarisation at E - and H -planes and so forth. Only few works focus on XPD of $\pm 45^\circ$ dual-polarised antennas. This is demonstrated in [10] for four horizontal parasitic elements that are added to a simple $\pm 45^\circ$ dual-polarised radiator to enhance XPD [10]. Unfortunately, horizontal parasitic elements enlarge the radiator's size (antenna excluding ground). The radiator's size in [10] is the square of the wavelength in free space. Therefore, larger element spacing is required when the proposed antenna is applied to base station array applications, which will lead to higher side-lobes. Only the XPD at boresight is presented for the antenna in [11]. The XPD of a vertical–horizontal dual-polarised antenna is studied in [12], but it differs from a $\pm 45^\circ$ dual-polarised antenna in terms of measuring techniques. Two parasitic elements are added in [13] to reduce the cross-polarisation of a patch antenna, but no explanation is provided as to why the parasitic elements reduce cross-polarisation. A 45° slant-polarised antenna is proposed in [14], but it is single-polarised and has an omnidirectional radiation pattern, which is not suitable for three-sector base station applications.

Circular polarisation (CP) can be radiated from a dual-polarised antenna when appropriate feed circuitry is provided. CP has been demonstrated to be a powerful tool in reducing multipath effects and offering flexibility in orientation angle between receiving and transmitting antennas. A CP antenna usually requires a wide 3 dB axial ratio (AR) beamwidth such that the wireless signal can be received from various angles.

Some techniques have been reported to widen the 3 dB AR beamwidth of basic CP antennas. Among them, parasitic square rings [15–18], circle rings [19, 20] or metal cylinders [21] are employed above or around a CP radiator to increase the AR beamwidth. Unfortunately, such approaches not only increase the overall size but also the complexity of CP antennas. Subsequently, the 3 dB AR beamwidth of CP radiation was widened by mechanically mounting a basic CP radiator on a three-dimensional square ground [22], a folded conducting wall [23], a pyramidal ground [24], a square conducting cavity [25] or a folded ground with three choke rings [26]. However, in addition to bulky geometry, these CP antennas suffer from certain difficulties in manufacturing the ground and assembling them with the basic CP radiator. By loading the top hats and mounting a reflector above and below crossed dipole antennas [27], a 140° 3 dB AR beamwidth was achieved at the cost of an enlarged height of $0.4\lambda_0$ (where λ_0 is the wavelength in free space). When planar CP antennas are comprised of two pairs of linear dipoles [28] or folded dipoles [29] in square contours, 126° or 135° 3 dB AR beamwidths, respectively, are obtained.

In this paper, a novel method is presented to improve the XPD of a broadband $\pm 45^\circ$ dual-polarised base station antenna within $\pm 60^\circ$ of the main lobe in the horizontal plane. Four vertical parasitic elements are placed between the ground and a $\pm 45^\circ$ dual-polarised base station antenna. Our results demonstrate that high XPD at broadside can be achieved by selecting suitable values for the position and length of the vertical parasitic elements. These elements form a substantial part of a novel dual-polarised base station antenna and increase XPD by about 7 dB at $\pm 60^\circ$. The antenna is designed, fabricated and measured. Experimental results are in good agreement with simulations and verify high XPD values owing to the addition of vertical parasitic elements. One of the advantages of this design is the size of the radiator; it is only $0.4\lambda_0 \times 0.4\lambda_0$, which is much smaller than that in [10] and thus is suitable for base station array applications. Moreover, with a broadband quadrature hybrid, the proposed antenna radiates CP and, because of the addition of vertical parasitic elements, the 3 dB AR beamwidth is widened from 84° to 195° .

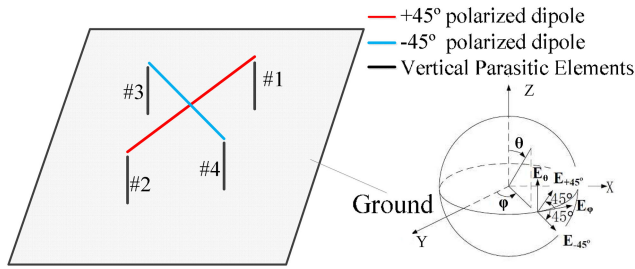


Fig. 1 Schematic of the proposed $\pm 45^\circ$ dual-polarised base station antenna with four vertical parasitic elements

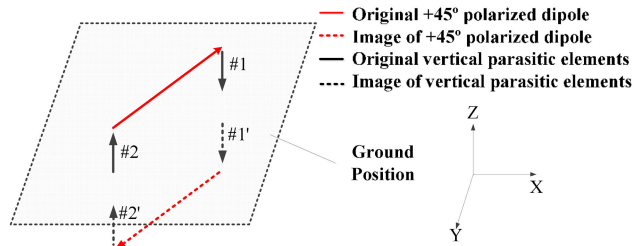


Fig. 2 Current distributions when $+45^\circ$ dipole is excited

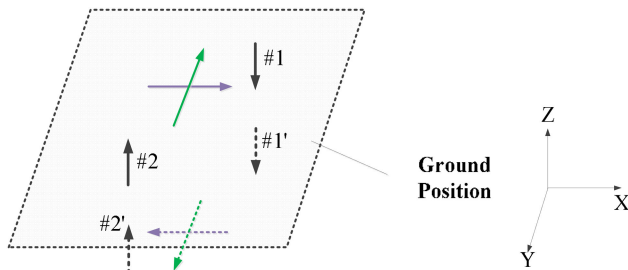


Fig. 3 Current decomposition associated with Fig. 2

	Radiation pattern of a horizontal dipole		Radiation pattern of a point source over a big reflector		Product of radiation patterns
$ E_\theta $		\times		$=$	

Fig. 4 Radiation pattern of a dipole parallel to Y-axis in the xz -plane

2 Diagonally dual-polarised base station antenna with enhanced XPD

Fig. 1 depicts a schematic diagram of the proposed $\pm 45^\circ$ dual-polarised base station antenna with four vertical parasitic elements. The ground is placed in the xy -plane. A $+45^\circ$ polarised dipole (between #1 and #2) and a -45° polarised dipole (between #3 and #4) are located above ground parallel to the xy -plane. The four parasitic elements (#1–#4) are located between the dipoles and the ground and are vertical to the xy -plane. E_θ and E_ϕ are the θ and ϕ components of the far-zone electric field, respectively. The current distributions of the antenna, when only the $+45^\circ$ polarised dipole is excited, are shown in Fig. 2. Since the -45° polarised dipole and parasitic elements #3 and #4 are located in a plane orthogonal to the $+45^\circ$ polarised dipole, no currents are induced. Thus, only images of the two vertical parasitic elements (#1 and #2) and the $+45^\circ$ polarised dipole need to be considered as shown in Fig. 2. The images of the parasitic elements are in phase with the original parasitic elements whereas the image of the $+45^\circ$ polarised dipole is out of phase with the original $+45^\circ$ polarised dipole.

	Radiation pattern of a horizontal dipole		Radiation pattern of a point source over a big reflector		Product of radiation patterns
$ E_\theta $		\times		$=$	

Fig. 5 Radiation pattern of a dipole parallel to X-axis in the xz -plane

	Radiation pattern of a monopole		Radiation patterns of an out-phase binary array		Product of radiation pattern
$ E_\theta $ (vertical parasitic elements)		\times		$=$	

Fig. 6 Radiation pattern of vertical parasitic elements in the xz -plane

$ E_\theta $				$=$	
$ E_\theta $		$+$		$=$	

Fig. 7 Graphical demonstration of realisation of identical radiation patterns in the xz -plane used for the proposed antenna in Fig. 1

The $+45^\circ$ polarised dipole can be decomposed into its x and y components as shown in Fig. 3. As discussed in [10], XPD, as a function of polar angle θ , can be calculated as

$$\text{XPD}(\theta) = 20 \times \log_{10} \left(\frac{E_{+45^\circ}(\theta)}{E_{-45^\circ}(\theta)} \right) \quad (1)$$

To obtain high XPD over a wide-angle range, the magnitudes and phases of E_θ and E_ϕ must be equal within the beamwidth. In the xz -plane, the beamwidth of E_ϕ is determined by the dipole oriented in y direction, and the beamwidth of E_θ is determined by both, the dipole oriented in x direction and the vertical parasitic elements. Radiation patterns of the dipoles oriented in x and y directions are shown in Figs. 4 and 5, respectively. The radiation pattern of the dipole in y direction is O-shaped, whereas the pattern of the dipole in x direction is figure-8-shaped. Since the products of patterns of the two dipoles are not identical, high XPD over a wide-angle range is difficult to achieve.

The radiation patterns of the vertical parasitic elements are shown in Fig. 6 where the parasitic elements are treated as monopoles. The currents of the two parasitic elements are out of phase. Thus, the total pattern of the two parasitic elements looks like the horizontal upper half of a figure-8-shape.

The pattern of E_θ is the summation of the patterns of the vertical parasitic elements and the dipole oriented in x direction.

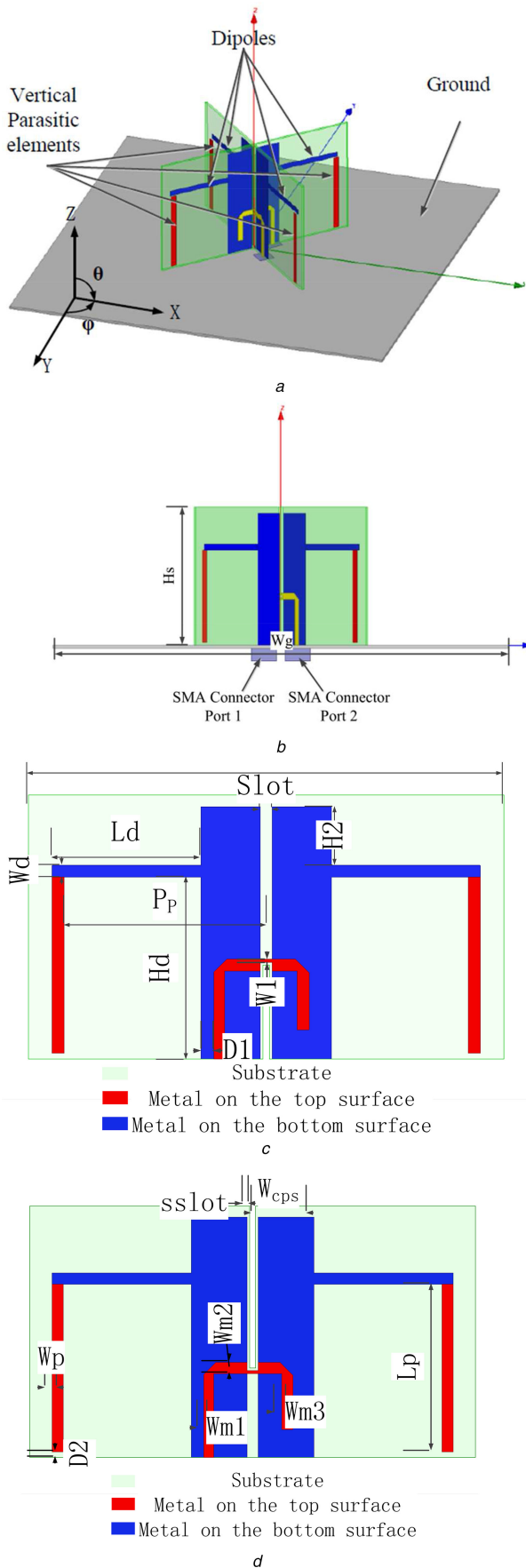


Fig. 8 Geometry of a simple ± 45 dual-polarised base station antenna with four parasitic elements
 (a) Three-dimensional view, (b) Side view (yz -plane), (c) $+45^\circ$ polarised element, (d) -45° polarised element

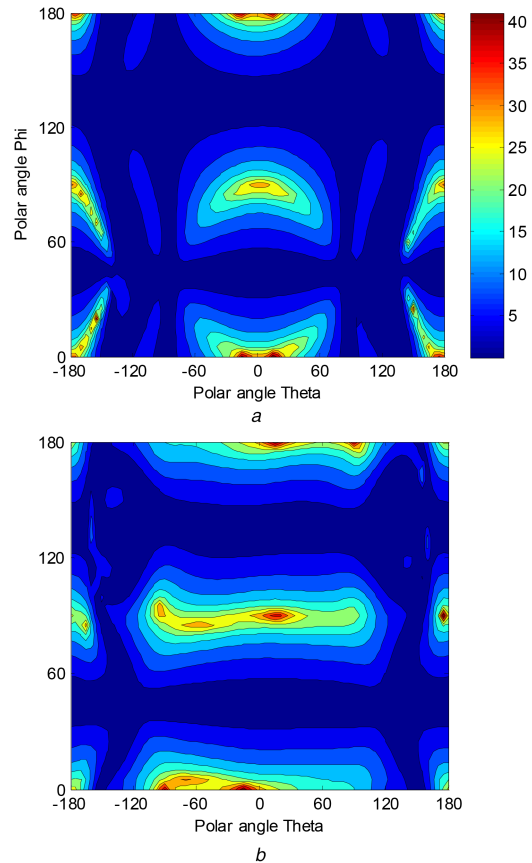


Fig. 9 Simulated XPDs for all polar angles when port 1 is excited
 (a) Without vertical parasitic elements, (b) With parasitic elements

Without the vertical parasitic elements, the beamwidth of E_θ is narrower than that of E_ϕ . After addition of the parasitic elements, the beamwidth of E_θ becomes wider and very similar to the one of E_ϕ as shown in Fig. 7. Therefore, high XPD within a wide beamwidth can be achieved.

The patterns in Figs. 4–7 are calculated with infinite ground plane, but we can only use finite ground plane. The radiation patterns with big finite ground plane are a bit different from the one with infinite ground plane, but principle described in Figs. 4–7 is still feasible.

Based on this discussion, a $\pm 45^\circ$ dual-polarised base station antenna, with improved XPD, is proposed as shown in Fig. 8 with all dimensional parameters tabulated in Table 1. The antenna is printed on Rogers 4003C substrate with relative permittivity of $\epsilon_r = 3.55$ and thickness of 0.813 mm. The operating frequency band of the antenna is 1.71–2.17 GHz. The effects of the vertical parasitic elements on XPD are displayed in Table 2. It is observed that without the parasitic elements, XPDs at $\pm 60^\circ$ of the polar angle θ are lower than 10 dB at some frequencies, and the minimum is 6.6 dB. However, with the added parasitic elements, XPD is obviously enhanced, and the minimum in the desired band increases to 15.2 dB. XPDs for all polar angles, when port 1 is excited, are shown in Fig. 9. It is observed that the XPDs have been enhanced in most polar angles. Integrated balun features are utilised to improve impedance matching over a wide frequency band as illustrated in [30].

To understand how the vertical parasitic elements affect the XPD performances, a parametric study is undertaken using Ansys HFSS. The results provide useful guidelines for practical designs.

Two factors mainly affect the XPD: first, the length of the vertical parasitic elements (L_p) and second, the position of the vertical parasitic elements (P_p). Table 3 shows XPDs of the two ports versus different lengths of L_p when one port is excited and the other one terminated. When the length of L_p is as short as 20 mm, XPDs are low and then increase with L_p . When $L_p = 28$ mm, XPDs are higher than 15 dB at all frequencies and all angles within $\pm 60^\circ$

of the main lobe. When L_p increases beyond 28 mm, XPDs decrease again.

XPDs versus different values of P_p are listed in Table 4. When P_p is as large as 42 mm, XPDs are low. With P_p decreasing, XPDs increase and are higher than 15 dB at all frequencies and all angles within $\pm 60^\circ$ of the main lobe when $P_p = 34$ mm. Further reduction of P_p results in decreasing XPDs. Therefore, $L_p = 28$ mm and $P_p = 34$ mm are selected in this design to obtain high XPD.

To verify the proposed design, a prototype is fabricated and measured. A photograph of the fabricated antenna is shown in Fig. 10. Radiation patterns in the xz -plane with one port excited and the other one terminated are depicted in Fig. 11. The measured patterns are in good agreement with simulations, and low cross-polarisation is obtained.

The XPD of the two ports is shown in Table 5. In the desired band of 1.71–2.17 GHz, the improved XPD is better than 25 dB at boresight and better than 14.7 dB within $\pm 60^\circ$ of the main lobe at the horizontal plane. These values are significantly higher than current technical standards of XPD.

The simulated and measured voltage standing wave ratios (VSWRs) and gains of the proposed antenna are shown in Fig. 12a. In the desired band, VSWRs better than 2 are achieved at both ports, and the gain of the antenna is 7 ± 1 dBi. Note that the gain decreases with frequency which is due to the fact that the currents on parasitic element become stronger and make the beamwidth wider and the gain lower. The measured isolation between the two ports, $|S_{21}|$ (Fig. 12b), indicates that in the band of interest, isolation is better than 30 dB.

Table 1 Dimensional parameters of the proposed antenna in Fig. 8

Parameter	Hs	Wg	Ls	Slot	Hd	Wd	Ld
value, mm	45	150	80	2	31	2	25
parameter	W1	sslot	Wcps	Wp	Lp	Wm1	D1
value, mm	0.5	1	10	2	31	1.8	2.2
parameter	H2	Wm2	P_p	D2	Wm3		
value, mm	10	2	34	1	2		

Table 2 Effect of vertical parasitic elements on XPD (unit: dB)

	Port 1					
	0° Without vertical parasitic elements	0° With vertical parasitic elements	-60° Without vertical parasitic elements	-60° With vertical parasitic elements	60° Without vertical parasitic elements	60° With vertical parasitic elements
1.7 GHz	27.0	30.5	6.6	17.3	8.5	19.2
1.95 GHz	32.5	31.6	8.8	22.9	9.5	22.6
2.2 GHz	31.8	30.5	11.0	16.9	11.3	16
	Port 2					
1.7 GHz	30.2	30.6	9.0	22.4	8.3	22.5
1.95 GHz	32.1	31.4	9.4	30.5	10.0	29.3
2.2 GHz	33.2	36.2	10.8	16.4	12.0	15.2

Table 3 XPD in the xz -plane versus different length of L_p (unit: dB)

		Port 1			Port 2		
		0°	+60°	-60°	0°	+60°	-60°
$L_p = 20$ mm	1.7 GHz	27.2	9.8	8.2	31.4	9.7	10.4
	1.95 GHz	32.8	11.7	10.9	32.7	12.0	11.8
	2.2 GHz	32.0	15.9	14.8	35.1	16.1	15.6
$L_p = 28$ mm	1.7 GHz	30.4	19.6	17.0	30.3	23.1	21.8
	1.95 GHz	31.4	23.3	23.4	30.4	31.5	28.7
	2.2 GHz	30.5	15.8	16.3	33.3	15.0	16.0
$L_p = 36$ mm	1.7 GHz	31.7	16.3	23.9	27.8	16.3	21.1
	1.95 GHz	29.2	14.0	14.1	29.5	13.1	12.9
	2.2 GHz	47.6	6.4	6.4	39.1	6.1	6.1

Table 4 XPDs in the xz -plane versus different value of P_p (unit: dB)

		Port 1			Port 2		
		0°	+60°	-60°	0°	+60°	-60°
$P_p = 26$ mm	1.7 GHz	29.9	16.5	14.5	30.7	18.4	18.2
	1.95 GHz	32.2	20.3	18.5	30.6	23.2	21.5
	2.2 GHz	30.3	17.9	19.2	33.2	16.5	18.9
$P_p = 34$ mm	1.7 GHz	30.5	19.6	17.0	30.3	23.1	21.8
	1.95 GHz	31.4	23.2	23.4	30.4	31.5	28.7
	2.2 GHz	30.4	15.8	16.3	33.4	15.0	16.0
$P_p = 42$ mm	1.7 GHz	27.3	11.6	9.7	31.2	11.5	12.4
	1.95 GHz	32.0	14.9	13.5	32.8	15.2	14.9
	2.2 GHz	31.8	25.8	19.4	35.0	23.7	21.8

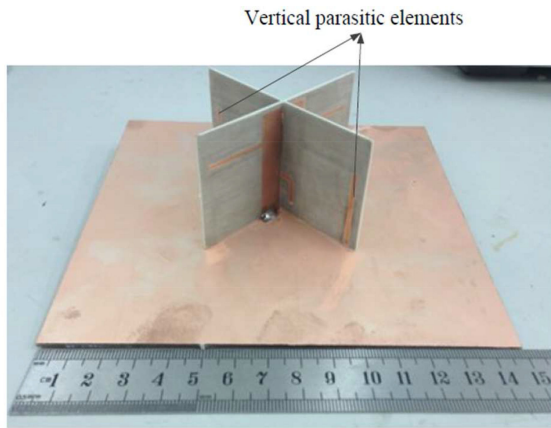


Fig. 10 Prototype of the proposed $\pm 45^\circ$ dual-polarised base station antenna

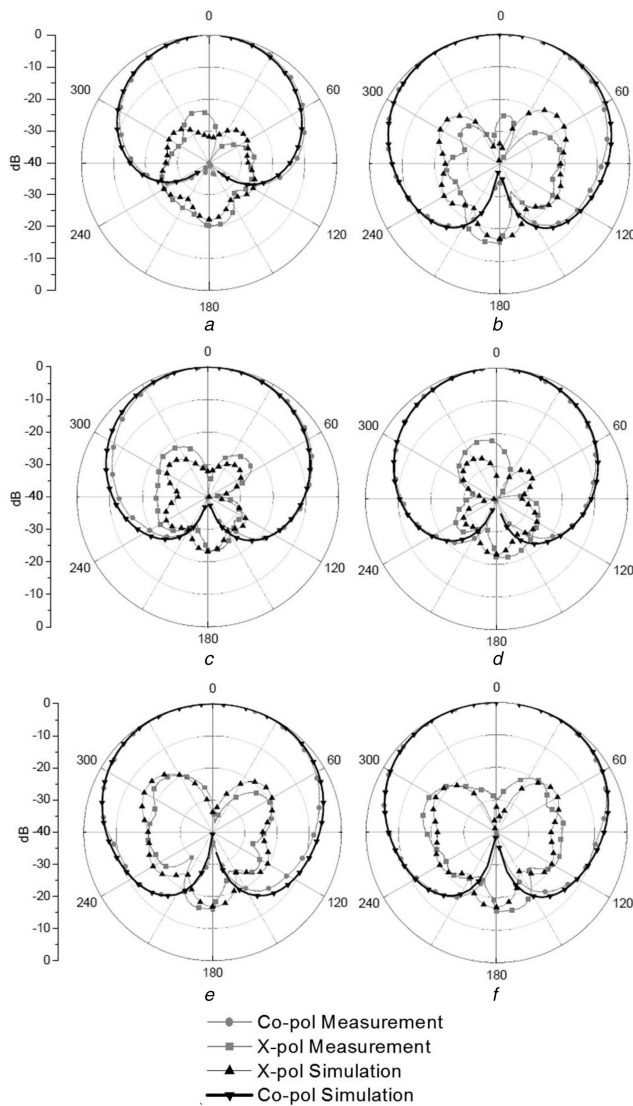


Fig. 11 Simulated and measured radiation patterns in xz -plane
(a) 1.7 GHz port 1, (b) 1.7 GHz port 2, (c) 1.95 GHz port 1, (d) 1.95 GHz port 2, (e) 2.2 GHz port 1, (f) 2.2 GHz port 2

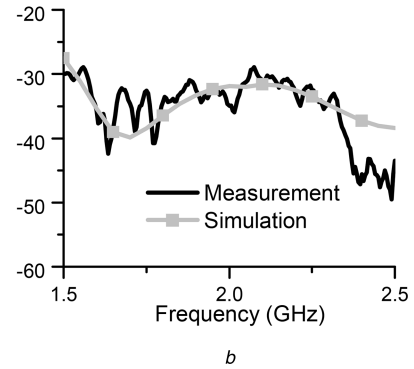
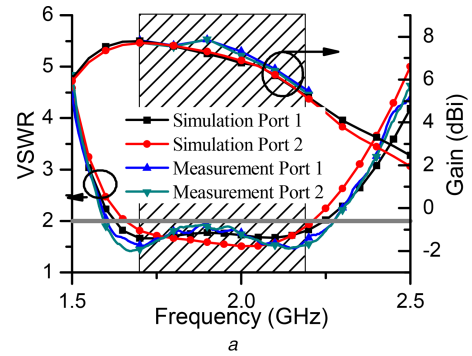


Fig. 12 Simulated and measured antenna parameters as a function of frequency
(a) Gain and VSWR, (b) Isolation between two ports

3 Circularly polarised base station antenna with enhanced AR beamwidth

If a dual-polarised antenna is excited with the same amplitude and a 90° phase difference, the phase difference between E_θ and E_ϕ is 90° and CP is produced. The AR at any polar angle θ can be expressed as

$$AR(\theta) = 120 \times \log_{10} \left| \frac{E_\theta(\theta)}{E_\phi(\theta)} \right| \quad (2)$$

As discussed in [28], to achieve a wide AR beamwidth, the following two conditions must be satisfied: first, the two elements are excited with the same magnitude and a 90° phase difference and, second, the magnitudes and phases of E_θ and E_ϕ must be equal over a wide beamwidth. According to the discussion in Section 2, the addition of the vertical parasitic elements leads to very similar E_θ and E_ϕ patterns. Therefore, we can predict that the vertical parasitic elements support a wide AR beamwidth.

To excite the proposed dual-polarised antenna with CP, a broadband quadrature hybrid is designed, fabricated and measured as displayed in Fig. 13. The quadrature hybrid is printed on substrate with the relative permittivity of $\epsilon_r = 2.55$ and the thickness of 0.8 mm.

Due to the symmetry of the antenna, only the radiation characteristics in the xz -plane are investigated in this work. The effects of the vertical parasitic elements on the AR beamwidth are shown in Fig. 14. The simulations demonstrate that without the parasitic elements, the 3 dB AR beamwidth is only 84° of the polar angle θ at the centre frequency of 1.95 GHz. After the addition of the vertical parasitic elements, the 3 dB AR beamwidth at the centre frequency is broadened to 215° , which confirms our

Table 5 Measured XPD of the proposed $\pm 45^\circ$ dual-polarised base station antenna (dB)

Frequency, GHz	Port 1			Port 2		
	0°	$+60^\circ$	-60°	0°	$+60^\circ$	-60°
1.7	25.03	23.19	21.45	31.69	23.24	24.82
1.95	35.24	20.69	16.03	29.29	20.95	23.43
2.2	31.7	16.19	17.14	28.37	14.72	19.8

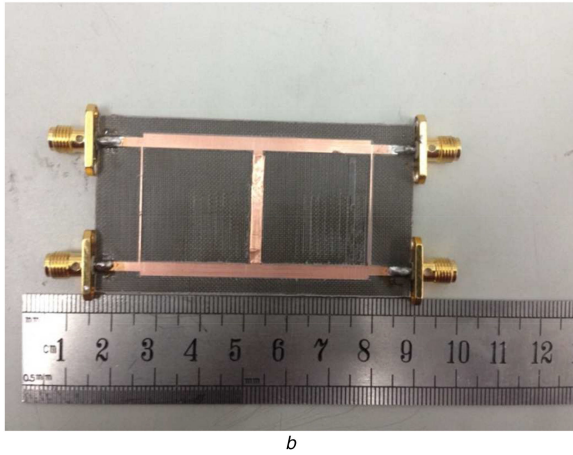
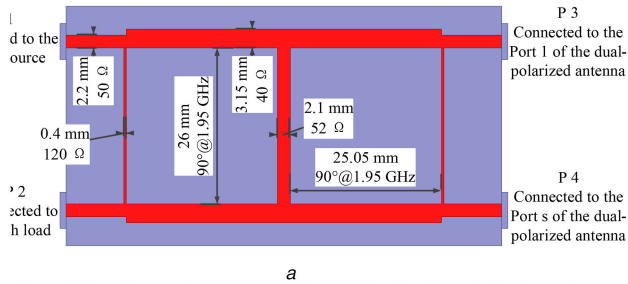


Fig. 13 Broadband quadrature hybrid for CP antenna
(a) Dimensions and equivalent circuits, (b) Photograph of the printed quadrature hybrid

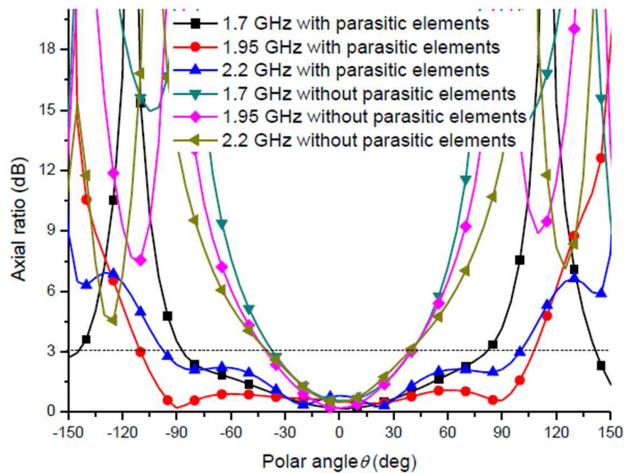


Fig. 14 Effects of vertical parasitic elements on AR beamwidth in the xz -plane

previous prediction. Moreover, the vertical parasitic elements widen the 3 dB gain beamwidth since with the addition of the parasitic elements, the 3 dB gain beamwidth is broadened by 20° (from 70° to 90°) at the centre frequency.

To excite the proposed CP antenna, a quadrature hybrid is employed as feed network for the CP antenna. Fig. 15 compares the simulated and measured ARs as a function of polar angle θ at 1.7, 1.95, and 2.2 GHz. Good agreement is observed over a wide angular range. The measured 3 dB AR beamwidth at the centre frequency of 1.95 GHz is 195° of the polar angle θ , i.e. between -98° and $+97^\circ$, as predicted. The measured radiation patterns are presented in Fig. 16 and verify the low AR values over a wide beamwidth. Finally, Fig. 17a presents the measured gain and AR as a function of frequency in broadside direction. In the desired band of 1.71–2.17 GHz, the AR is <1.5 dB and gain is 4.3 dBi with 1.2 dBi variation. The measured VSWR values of the overall CP antenna (dipole plus hybrid) are shown in Fig. 17b. In the desired band, the VSWR is better than 1.25.

Finally, although the proposed antenna is completely symmetric, radiation patterns, AR and XPD plots show slight

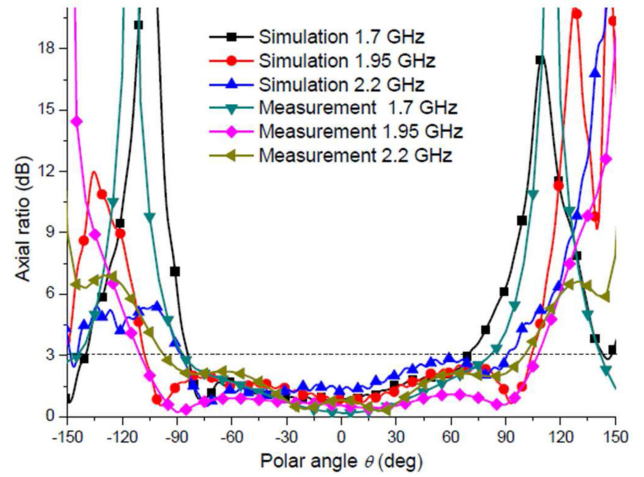


Fig. 15 Simulated and measured AR of the CP antenna in the xz -plane

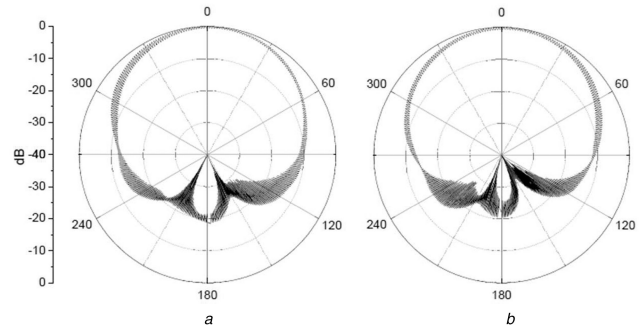


Fig. 16 Measured radiation patterns of the proposed CP antenna at 1.95 GHz
(a) xz -plane, (b) yz -plane

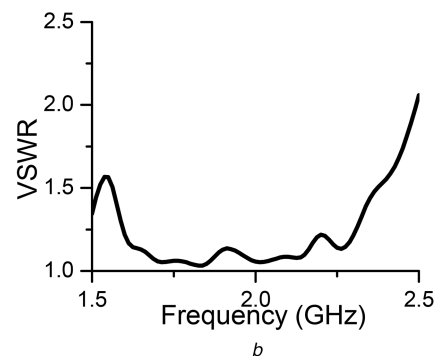
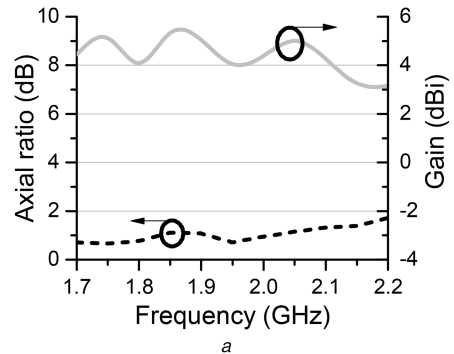


Fig. 17 Measured CP antennas parameters as a function of frequency
(a) AR and gain, (b) VSWR of the overall CP antenna

asymmetries. This is due to the fact that the feeding microstrip lines render the entire structure asymmetric.

4 Conclusion

The addition of four vertical parasitic elements to a diagonally dual-polarised base station antenna significantly improves XPD while maintaining a VSWR < 2. Measured results show that in the desired band of 1.71–2.17 GHz, XPD values can be achieved that are higher than 25 dB at boresight and better than 14.7 dB within $\pm 60^\circ$ of the main lobe in the horizontal plane. By adding a quadrature hybrid for CP radiation, the same antenna can be used to widen the 3 dB AR beamwidth up to 195° at the centre frequency. The proposed dual-polarised and CP antennas are good candidates for many modern wireless communication applications.

5 References

- [1] Vaughan, R.G.: 'Polarization diversity in mobile communications', *IEEE Trans. Veh. Technol.*, 1990, **39**, (3), pp. 177–186
- [2] Lempiainen, J.J.A., Laiho-Steffens, J.K.: 'The performance of polarization diversity schemes at a base station in small/micro cells at 1800 MHz', *IEEE Trans. Veh. Technol.*, 1998, **47**, (3), pp. 1087–1092
- [3] Ludwig, A.C.: 'The definition of cross-polarization', *IEEE Trans. Antennas Propag.*, 1973, **21**, (1), pp. 116–119
- [4] Cui, Y.H., Li, R.L., Fu, H.Z.: 'A broadband dual-polarized planar antenna for 2G/3G/LTE base stations', *IEEE Trans. Antennas Propag.*, 2014, **62**, (9), pp. 4836–4840
- [5] Gou, Y., Yang, S., *et al.*: 'A compact dual-polarized printed dipole antenna with high isolation for wideband base station applications', *IEEE Trans. Antennas Propag.*, 2014, **62**, (8), pp. 4392–4395
- [6] Luo, K., Ding, W., *et al.*: 'Design of dual-feed dual-polarized microstrip antenna with high isolation and low cross polarization', *Prog. Electromagn. Res. Lett.*, 2013, **36**, pp. 31–40
- [7] Li, B., Yin, Y.Z., *et al.*: 'Dual-polarised patch antenna with low cross-polarisation and high isolation for WiMAX applications', *IET Electron. Lett.*, 2011, **47**, (17), pp. 592–593
- [8] Li, M., Luk, K.M.: 'Wideband magnetoelectric dipole antennas with dual polarization and circular polarization', *IEEE Antennas Propag. Mag.*, 2015, **57**, (1), pp. 110–119
- [9] Zuo, S., Liu, Q.Q., Zhang, Z.Y.: 'Wideband dual-polarized crossed-dipole antenna with parasitical crossed-strip for base station applications', *Prog. Electromagn. Res. C*, 2014, **48**, pp. 159–166
- [10] Luo, Y., Chu, Q.-X., Wen, D.-L.: 'A $\pm 45^\circ$ dual-polarized base-station antenna with enhanced cross-polarization discrimination via addition of four parasitic element placed in a square contour', *IEEE Trans. Antennas Propag.*, 2016, **64**, (4), pp. 1514–1519
- [11] Kaboli, M., Abrishamian, M.S., *et al.*: 'High-isolation XX-polar antenna', *IEEE Trans. Antennas Propag.*, 2012, **60**, (9), pp. 4046–4055
- [12] Oh, T., Lim, Y.G., *et al.*: 'Dual-polarization slot antenna with high cross polarization discrimination for indoor small-cell MIMO system', *IEEE Antennas Wirel. Propag. Lett.*, 2015, **14**, pp. 374–377
- [13] Waterhouse, R.: 'Printed antennas for wireless communications' (John Wiley & Sons, New York, 2007), p. 247
- [14] Quan, X.L., Li, R.L., *et al.*: 'Analysis and design of a 45° slant-polarized omnidirectional antenna', *IEEE Trans. Antennas Propag.*, 2014, **62**, (1), pp. 86–93
- [15] Latif, S.I., Shafai, L.: 'Hybrid perturbation scheme for wide angle circular polarisation of stacked square-ring microstrip antenna', *IET Electron. Lett.*, 2007, **43**, (20), pp. 1065–1066
- [16] Latif, S.I., Shafai, L.: 'Circular polarisation from dual-layer square-ring microstrip antennas', *IET Microw. Antennas Propag.*, 2012, **6**, (1), pp. 1–9
- [17] Navarro, V., Carrera, F., Baquero, M.: 'Circular polarization patch antenna with low axial ratio in a large beamwidth'. Proc. 7th European Conf. Antennas Propagation, Gothenburg, Sweden, April 2013, pp. 3330–3333
- [18] Tan, T.-S., Xia, Y.-L., Zhu, Q.: 'A novel wide beamwidth and circularly polarized microstrip antenna loading annular dielectric superstrate with metal ring'. IEEE AP-S Int. Symp. Digest, Memphis, TN, July 2014, pp. 1883–1884
- [19] Choi, E.-C., Lee, J.W., Lee, T.-K.: 'An axial ratio beamwidth enhancement of S-band satellite antenna with parasitic elements and its arrays', *IEEE Antennas Wirel. Propag. Lett.*, 2014, **13**, pp. 1689–1692
- [20] Pan, Z.K., Lin, W.X., Chu, Q.X.: 'Compact wide-beam circularly polarized patch antenna with a parasitic ring for CNSS application', *IEEE Trans. Antennas Propag.*, 2014, **62**, (5), pp. 2847–2850
- [21] Liu, Q., Shen, J., *et al.*: 'Dual-band circularly-polarized unidirectional patch antenna for RFID reader applications', *IEEE Trans. Antennas Propag.*, 2014, **62**, (12), pp. 6428–6434
- [22] Tang, C.L., Chiou, J.Y., Wong, K.L.: 'Beamwidth enhancement of a circularly polarized microstrip antenna mounted on a three-dimensional ground structure', *Microw. Opt. Technol. Lett.*, 2002, **32**, (2), pp. 149–153
- [23] Nakano, H., Shimada, S., *et al.*: 'Circularly polarized patch antenna enclosed by a folded conducting wall'. Proc. IEEE Topical Conf. Wireless Communications Technology, Honolulu, USA, October 2003, pp. 134–135
- [24] Su, C.W., Huang, S.K., Lee, C.H.: 'CP microstrip antenna with wide beamwidth for GPS band application', *IET Electron. Lett.*, 2007, **43**, (20), pp. 1062–1063
- [25] Ye, X., He, M., *et al.*: 'A compact single-feed circularly polarized microstrip antenna with symmetric and wide-beamwidth radiation pattern', *Int. J. Antennas Propag.*, 2013, **2013**, (7), pp. 1–7
- [26] Duan, X.-D., Li, R.-L.: 'A novel center-fed dual-band circularly polarized antenna for GNSS application'. IEEE AP-S Int. Symp. Digest, Memphis, USA, July 2014, pp. 1015–1016
- [27] Ta, S.X., Park, I., Ziolkowski, R.W.: 'Dual-band wide-beam crossed asymmetric dipole antenna for GPS applications', *IET Electron. Lett.*, 2012, **48**, (25), pp. 1580–1581
- [28] Luo, Y., Chu, Q.-X., Zhu, L.: 'A low-profile wide-beamwidth circularly-polarized antenna via two pairs of parallel dipoles in a square contour', *IEEE Trans. Antennas Propag.*, 2015, **63**, (3), pp. 931–936
- [29] Luo, Y., Chu, Q.-X., Zhu, L.: 'A miniaturized wide-beamwidth circular polarized planar antenna via two pairs of folded dipoles in a square contour', *IEEE Trans. Antennas Propag.*, 2015, **63**, (8), pp. 3753–3759
- [30] Li, R.L., Wu, T., *et al.*: 'Equivalent-circuit analysis of a broadband printed dipole with adjusted integrated balun and array for base station applications', *IEEE Trans. Antennas Propag.*, 2009, **57**, (7), pp. 2180–2184